Bistability of bursting and silence regimes in a model of a leech heart interneuron

Tatiana Malashchenko, Andrey Shilnikov, and Gennady Cymbalyuk
Neuroscience Institute, Georgia State University, 100 Piedmont Avenue SE, Atlanta, Georgia 30303, USA
(Received 27 August 2010; revised manuscript received 3 May 2011; published 10 October 2011)

Bursting is one of the primary activity regimes of neurons. Our study is focused on determining a generic biophysical mechanism underlying the coexistence of the bursting and silent regimes observed in a neuron model. We show that the main ingredient for this mechanism is a saddle periodic orbit. The stable manifold of the orbit sets a threshold between the regimes of activity. Thus, the range of the controlling parameters, where the coexistence is observed, is limited by the bifurcations' values at which the saddle orbit appears and disappears. We show that it appears through the subcritical Andronov-Hopf bifurcation, where the equilibrium representing the silent regime loses stability, and disappears at the homoclinic bifurcation. Correspondingly, the bursting regime disappears in close proximity to the homoclinic bifurcation.

DOI: 10.1103/PhysRevE.84.041910 PACS number(s): 87.19.ll, 05.45.−a

I. INTRODUCTION

Cardiac cells and a variety of neurons have been shown to exhibit bistability [1–5]. Certain perturbations of the state of a bistable excitable cell may trigger a switch between two coexisting regimes of activity, such as, for example, periodic spiking and silence in a cardiac cell [5], and in the squid giant axon [6]. The mechanisms supporting multistability in excitable cells are not well understood. The more such mechanisms we know, the closer we will be to applying this knowledge to the development of biofeedback stimulation treatments that could prevent the onset of pathological regimes such as seizures, by inducing a switch back to a normal regime [7–10]. Analysis of the dynamical mechanisms supporting bistability is facilitated by the appropriate choice of an invertebrate model system [11]. Such a system allows the investigation of bistability on a cellular level using identified neurons [6,12,13]. For example, the hand-in-hand modeling of and experiments on the neuron R15 from the mollusk Aplysia demonstrated the bistability of bursting and tonic spiking [12,14]. Another classical example of such a system is the celebrated squid giant axon made famous by the studies of ionic currents by Hodgkin and Huxley [15]. These two components—first, having a neuron that is identified so that a researcher can always find it from preparation to preparation; and, second, having a biophysically accurate model that describes the dynamics of these regimes—make it no surprise that it is the number one system where the bistability of tonic spiking and silence is studied with an exemplary thoroughness. These studies have made the coexistence of tonic spiking and silence into probably the most extensively studied type of bistability [6,16–19]. In a striking contrast, there is a gap in our knowledge when it comes to understanding the mechanisms supporting the bistability of bursting and silence in the dynamics of a single neuron. In this work we describe the mechanism producing bistability in the leech heart interneuron.

Several different classes of neurons displayed the coexistence of tonic spiking and silence [1,3,4]. The coexistence of regimes implies that their basins of attraction are separated by a barrier created by an unstable regime. The mechanisms supporting bistability can be classified in terms of the unstable regime involved. Models exhibiting coexistence of tonic spiking and silence usually have either a saddle equilibrium or saddle periodic orbit involved. A stable manifold of a saddle separates the rest state and tonic spiking, setting a threshold between these two attractors. Purkinje cells and motoneurons were shown to exhibit the type of bistability based on a saddle equilibrium [4,20]. The Hodgkin-Huxley model has bistability based on a saddle periodic orbit [19].

The saddle periodic orbit commonly appears through the subcritical Andronov-Hopf bifurcation, which is a ubiquitous cause of bistability in different nonlinear systems. In the Hodgkin-Huxley model a saddle orbit terminates at a saddle-node bifurcation for periodic orbits, at which the stable and unstable periodic orbits coalesce and disappear. The bifurcations that determine the appearance and disappearance of the unstable periodic orbit limit the range of the control parameter values for which the bistability exists. This bistability investigated in the model has been clearly experimentally identified in the squid giant axon under low Ca^{2+} bath concentration; by applying a single current pulse to a squid axon the transition between tonic spiking and silence was shown [6]. The unstable oscillatory regime was recorded for several periods before the activity settled to one of the attracting regimes. This example unites experimental and theoretical studies and illustrates the advantages of studying the neuronal dynamics of identified neurons.

Motor control of rhythmic movements commonly employs specialized oscillatory neuronal networks, central pattern generators (CPGs) [11]. The leech heart beat CPG is one of the best studied invertebrate neuronal networks, with a clearly identified function, a set of identified participating neurons, and well-developed biophysically accurate models. It consists of a small number of interneurons distributed over several ganglia. Those located in ganglia 3 and 4 are responsible for generating basic rhythm [22]. Here we focus on the dynamics of a single interneuron from either ganglion 3 or 4. The predictions of this work could be tested in further studies since synaptic interaction within this CPG can be blocked pharmacologically [21,22]. These neurons are particularly attractive for analysis in terms of the theory of dynamical systems since their membrane ionic currents have been measured and well described by a canonical model using the Hodgkin-Huxley formalism [23]. The canonical model has proven itself as a powerful tool in predicting phenomena [23,24]. Depending on the value

of the parameters, the model can exhibit different regimes including tonic spiking, bursting, silence, and subthreshold oscillations. The bistability of bursting and silence has also been observed in this model [24] and the goal of this study is to describe the mechanism that supports it. We start by showing that the switch from silence to bursting activity can be achieved by current perturbation. We show the involvement of the unstable subthreshold oscillations; and with one-parameter bifurcation analysis we describe the origin and disappearance of the subthreshold oscillations. Finally, we performed two-parameter bifurcation analysis to show the range of leak current parameters where bistability can be observed.

II. RESULTS

We studied the dynamics of the canonical leech heart interneuron model. Bistability of bursting and silent regimes had been demonstrated previously [24], but the mechanism supporting it was not described. The model contained nine voltage-dependent currents: fast calcium current (I_{CaF}), slow calcium current (I_{CaS}), fast sodium current (I_{Na}), delayed rectifier-potassium current (I_{K1}), persistent potassium current (I_{K2}), fast transient potassium current I_{KA}, hyperpolarization activated cationic current (I_h), persistent sodium current (I_P), and leak current (I_{leak}) and was described by a system of 14 differential equations [23] (Appendix). The parameters of the canonical model were tuned to produce activity with a wave form close to the one experimentally observed [23,24]. The trajectories of this model were obtained using the Matlab ODE solver, ode15s. Absolute tolerance and relative tolerance were 10^{-9} and 10^{-8}. The integration and bifurcation analysis were performed using the software package CONTENT [25,26]. The integration of equations was done using the Runge-Kutta method of the fourth order with the tolerance of integration set as 10^{-9}. Bistability was reported in the model with elevated conductance of the leak current, g_{leak}.

We were able to elicit a switch from silence to bursting activity by applying a square pulse of current. The switch could be triggered by either a negative or positive pulse (Fig. 1). All parameters including E_{leak} were set to the canonical values, but g_{leak} was set to 10.7 nS; the canonical value is 9.9 nS [23,24]. The initial conditions of voltage and gating variables were set so that the model initially exhibited silence. We used square pulses with a duration of 0.03 sec. In Fig. 1(a) a hyperpolarizing pulse of current with the amplitude of 0.05 nA switched the activity from silence to the bursting regime. By trying different amplitudes of the pulse, we found that negative pulses within the range -0.0213 nA $< I_{inj} <$ 0.0 nA did not switch silence into the bursting regime, while negative pulses with an amplitude larger than 0.0213 nA did switch the activity. Perturbations of the initially silent neuron by the depolarizing square pulse of current showed that only a pulse with an amplitude larger than 0.0175 nA could switch the activity from silence to bursting. Figure 1(b) shows the example of perturbation by a positive pulse with the amplitude $I_{inj} =$ 0.05 nA. For a pulse duration of 0.03 sec, the critical values, $I_{inj} = -0.0213$ nA and $I_{inj} = 0.0175$ nA, set two thresholds for the amplitude of the pulse of current, I_{th}, for the switch from silence to bursting—negative and positive. Repeating this analysis we found the two thresholds for pulses with different durations (Fig. 2). The longer the duration of the pulses was, the smaller the two thresholds were. The two data sets obtained fit well to the empirical Lapicque strength-duration formula describing the property of the minimum strength pulse triggering a spike in an excitable cell [27–29]

$$I_{th} = \frac{I_{rheobase}}{1 - e^{T/\tau_m}},$$

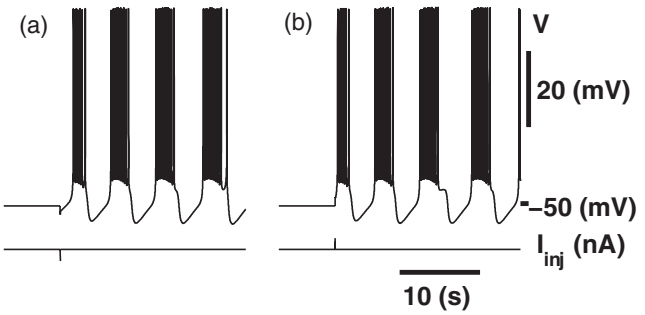

FIG. 1. Perturbation by a square pulse of current switches the regime of activity from silence into bursting. (a) A negative, hyperpolarizing pulse of current $I_{inj} = -0.05$ nA switches activity from silence to bursting. The minimum magnitude of I_{inj} that can induce the switch is –0.02131 nA. (b) A positive, depolarizing pulse of current $I_{inj} = 0.05$ nA also initiates the bursting activity. To switch the activity, I_{inj} has to be larger than the value of 0.0175 nA. For either polarity of the pulse, the pulse duration was 0.03 sec. The parameters of the leak current are $E_{leak} = -0.0635$ V and $g_{leak} = 10.7$ nS.

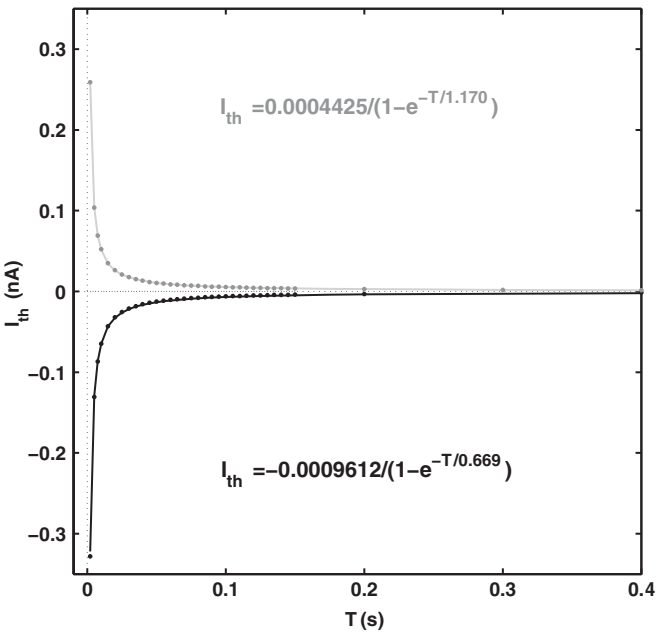

FIG. 2. The strength-duration relationships of the minimum depolarizing (gray) and hyperpolarizing (black) square pulses of current switching the silent regime into the bursting regime. To toggle the switch the pulse strength must be larger than the thresholds I_{th} determined by the relationships. The two data sets (dots) were obtained numerically and then fitted to the Lapicque formula (curves). The parameters of the leak current are the same as in Fig. 1.

where I_{rheobase} is the asymptotic current's threshold value for the infinitely long pulse, T is the pulse duration, and τ_m is a time constant characterizing the process of charging the cell's membrane.

Our previous study of the leech heart interneuron model showed that the bistability of bursting and silence is associated with the Andronov-Hopf bifurcation [24]. These results suggest that the separating barrier between the two attractors, bursting and silent, is the stable manifold of a saddle periodic orbit. The Lapicque formula approximates well the strength-duration relationship of a square pulse of current which is sufficient to move a phase point from the stable stationary state across the stable manifold into the basin of attraction of bursting activity.

A. The unstable orbit disappears at a homoclinic bifurcation

We investigated the stability of the equilibria of the model for $E_{\text{leak}} = -0.0635$ V. Evolution of the equilibria and their stability were analyzed with g_{leak} being varied as the bifurcation parameter in the CONTENT software. The plot of the membrane potential associated with each equilibrium versus the bifurcation parameter g_{leak} exhibits a z-shaped curve of the equilibria branches. This curve has two branches made of the equilibria, which are the hyperpolarized and depolarized rest states, separated by the saddle. First, we set a large value of g_{leak}, so that the model stayed at the stable hyperpolarized stationary state. We examined how the stability of the hyperpolarized equilibrium changed in response to a decrease in the bifurcation parameter g_{leak} (Fig. 3(a)). The hyperpolarized equilibrium lost its stability through the subcritical Andronov-Hopf bifurcation. For $E_{\text{leak}} = -0.0635$ V, the bifurcation occurred at $g_{\text{leak}}^{\text{AH}} = 10.67$ nS; and the stable rest state became a saddle focus. The subcritical Andronov-Hopf bifurcation (AH) gave rise to an unstable periodic orbit with zero amplitude and period 3.05 sec. As the bifurcation parameter g_{leak} was increased, the amplitude of the unstable orbit grew proportionally to $\sqrt{g_{\text{leak}} - 10.67}$ while g_{leak} was close to the bifurcation value $g_{\text{leak}}^{\text{AH}}$. As the parameter g_{leak} was increased further the unstable orbit approached the saddle located on the middle branch of the z-shaped curve. To depict this evolution of the orbit, we plotted the minimum, maximum and average values of the membrane potential of the unstable orbit against g_{leak} together with the z-shaped curve. In the vicinity of the saddle, the period of the orbit grew logarithmically fast. For the range of g_{leak} from 10.85 nS to 10.873 nS [Fig. 3(b)] the period of the orbit grew rapidly from 7 sec to 100 sec. The graph was fitted by the function $-1.198 \ln(|10.873 - g_{\text{leak}}|)$. Near $g_{\text{leak}} = 10.873$ nS the amplitude of the oscillations stayed constant while the period grew. At the value $g_{\text{leak}} = 10.873$ nS the homoclinic bifurcation (Hom) occurred in the system. Concerning the unstable subthreshold oscillations this analysis suggests that they could be recorded experimentally.

We compared the unstable periodic orbit obtained using the bifurcation analysis software CONTENT with those recorded after a square pulse of current with an amplitude that is very close to the threshold value. Let's consider again the canonical model with elevated leak conductance, $g_{\text{leak}} = 10.7$ nS. We

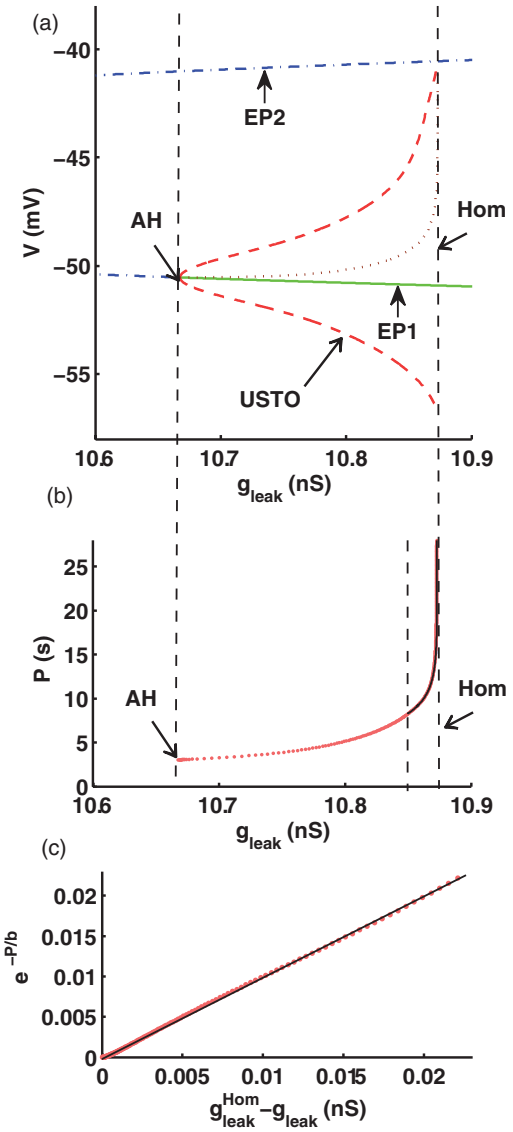

FIG. 3. (Color) Bifurcation diagram of the stationary states and hyperpolarized subthreshold oscillations of the model. (a) The solid green line represents the stable hyperpolarized equilibrium (EP1). Subcritical Andronov-Hopf bifurcation (AH) occurs at $g_{\text{leak}} = 10.67$ nS (marked by the left vertical dashed line, $E_{\text{leak}} = -0.0635$ mV) where the equilibrium loses its stability and gives rise to the unstable periodic orbit. For the values of g_{leak} smaller than this critical value the equilibrium is unstable (dashed blue line). The dashed blue line located above it depicts the saddle equilibria (EP2). The curve of the depolarized equilibrium has the membrane potential near +0.01 V and is not shown. The unstable periodic orbit corresponds to the unstable subthreshold oscillations (USTO). It is marked by the two dashed red curves and the dashed brown curve locating the minimum, maximum, and average values of the membrane potential of the oscillations correspondingly. The unstable orbit disappears at the homoclinic bifurcation (Hom), marked by the dashed vertical line at the right, $g_{\text{leak}} = 10.873$ nS. (b) Red dots graph the values of the period, P, of USTO as the g_{leak} is varied between the two bifurcation values. As the unstable periodic orbit approaches the homoclinic bifurcation the period grows as $-1.198 \ln(|10.873 - g_{\text{leak}}|)$ as shown by the blue curve. (c) Inset shows the part of the graph in (b) taken in the vicinity of the homoclinic bifurcation, where $b = 1.198$, $g_{\text{leak}}^{\text{Hom}} = 10.873$ nS.

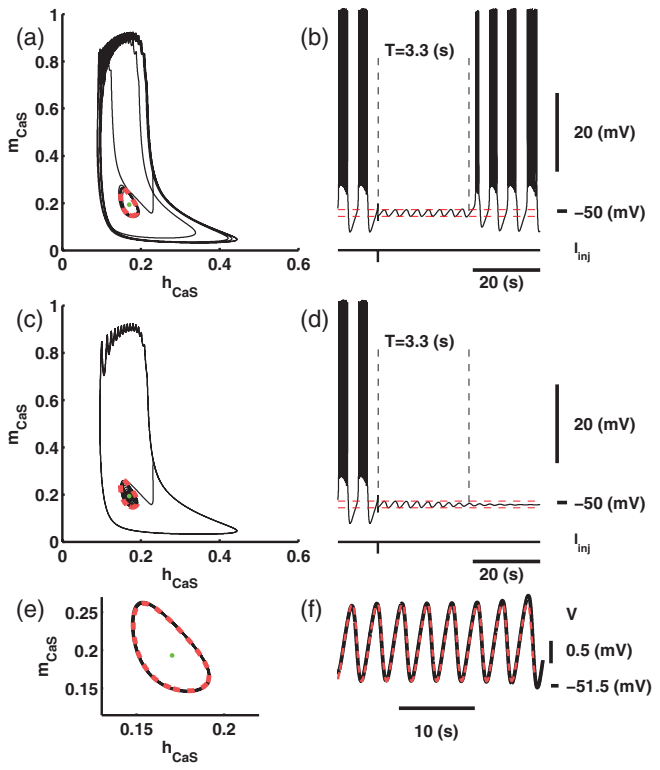

FIG. 4. (Color online) Coexistence of bursting and silence. The negative square pulse of I_{inj} perturbed the bursting activity. Bursting and transient activities are represented by black solid line. (a), (c), (e) Two-dimensional (2D) projection reveals unstable oscillations represented by dashed red (gray) loop along with the two attractors: the bursting and the hyperpolarized equilibrium, green (gray) dot. (a), (b) The pulse with the amplitude of −0.01044 nA moved the phase point toward the unstable periodic orbit, allowed recording the subthreshold oscillations for eight periods, but did not switch the activity from bursting into silence. (c), (d) The pulse with the amplitude −0.01045 nA again allowed recording the subthreshold oscillations for a few periods, moved the phase point into the basin of attraction of the equilibrium, thus producing the switch from bursting into the silence. The dashed red (gray) lines in plots (b) and (d) mark the minimum and maximum values of the membrane potential of the unstable orbit obtained with the bifurcation analysis. (e), (f) This is the part of the trajectory with the unstable oscillations (solid) revealed by the perturbation plotted together with the unstable periodic orbit (dashed). The parameters of the leak current were the same as in Fig. 1.

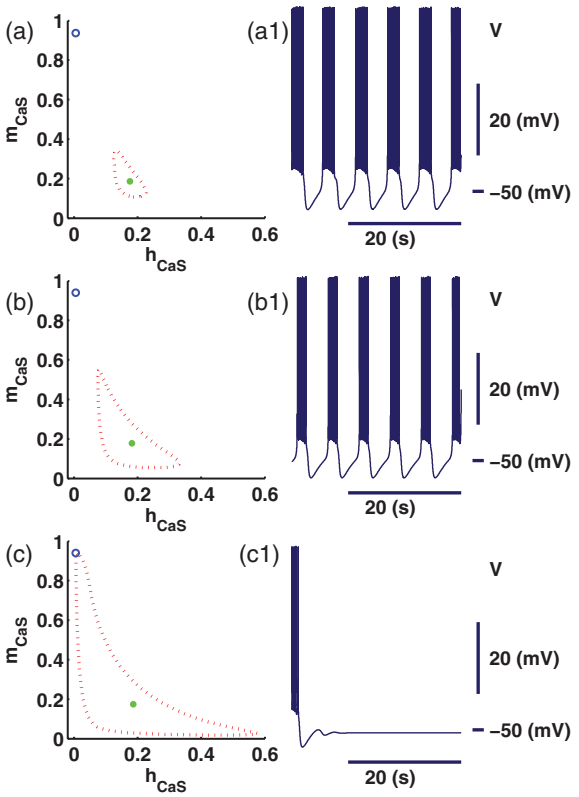

FIG. 5. (Color online) Bursting, the saddle orbit and silent regimes at different values of the controlling parameter g_{leak}. The saddle orbit, stable and saddle equilibria on the 2D projection onto (m_{CaS},h_{CaS}) plane presented for three g_{leak} values, 10.76 nS (a), 10.83 (b), 10.87 (c); and panels (a1), (b1), (c1) show corresponding bursting activities. On panels (a), (b), and (c), the saddle orbit is marked by the dashed loop; and the stable and the saddle equilibrium are shown by the filled green (gray) and open blue (gray) circles, correspondingly. The homoclinic bifurcation occurs at $g_{leak} = 10.873$ nS, where the saddle orbit merges with the saddle equilibrium. Panels (a1) and (b1) show the bursting activities of the models such that in parameter space one is relatively far from the bifurcation [(a1)] and the other is close to the transition from bursting to silence [(b1)]. Both cases exhibit the bistability of bursting and silence. At the parameter value close to the bifurcation [(c), (c1)], bursting no longer exists as a regime; and silence is the only attractor [(c1)]. The value of E_{leak} was −0.0635 V for all the plots.

set the initial conditions that corresponded to the bursting regime. With these initial conditions the model would exhibit bursting indefinitely; to confirm that the bursting regime is the attractor, the system was integrated for several thousand seconds. To perform the switch from bursting to silence, we applied a negative pulse of current near the first spike of a burst. Pulses with an amplitude of the current pulse close to −0.010445 nA revealed unstable subthreshold oscillations for several periods [Figs. 4(b) and 4(d)]. Now we plotted together the saddle periodic orbit obtained with the parameter continuation software CONTENT for $g_{leak} = 10.7$ nS and the subthreshold oscillations recorded after the pulse [Figs. 4(e) and 4(f)]. The unstable periodic orbit is presented by dashed red (gray) curve. The trajectory of the unstable subthreshold oscillations is extracted from the trace in Fig. 4(b) between two vertical lines and is shown by black curve in Figs. 4(e) and 4(f) (inset). Minimum and maximum voltages of the unstable periodic orbit are also plotted in Figs. 4(b) and 4(d). The two trajectories appeared very close to each other when projected on the plane created by the state variables gating the conductance of the slow calcium current [Fig. 4(e)] and also plotted as membrane potentials versus time [Fig. 4(f)]. Figure 4 illustrates the position of the unstable periodic orbit relative to rest state and bursting trajectory projected onto the plane (m_{CaS},h_{CaS}). It allows one to observe how a pulse of current brings the phase point of the bursting trajectory into the basin of attraction to the rest state, which is separated by the stable manifold of the saddle periodic orbit.

As we elevated g_{leak} in small increments the saddle orbit grew in size approaching the saddle rest state [Figs. 5(a)–5(c)]. By tracing the bursting activity for the same values of g_{leak}, we found that the transition from bursting to silence occurred very close to but slightly before the homoclinic bifurcation [Figs. 5(a1)–5(c1)]. The wave form of the bursting activity changed only slightly as the controlling parameter was set closer and closer to the transition value. At $g_{leak} = 10.87$ nS the bursting activity was not observed and the stable stationary state was the only attractor. Up to the transition point the neuron exhibited bistability.

To summarize, the unstable periodic orbit appears through the subcritical Andronov-Hopf bifurcation and disappears at the homoclinic bifurcation. The orbit corresponds to unstable subthreshold oscillations, which could be revealed by a pulse of current. The homoclinc bifurcation bounds the range where the bursting regime could exist, since the separating saddle regime does not exist beyond the bifurcation value.

We numerically computed a two-parameter bifurcation diagram of oscillatory and stationary regimes (Fig. 6). The range of the parameters of the leak current (g_{leak}, E_{leak}) supporting bursting activity has a banana shape and is surrounded by a large area supporting tonic spiking activity on the left side and a silent regime on the right side. The borders between regimes are associated with bifurcations in the system. The period-doubling bifurcation of the stable

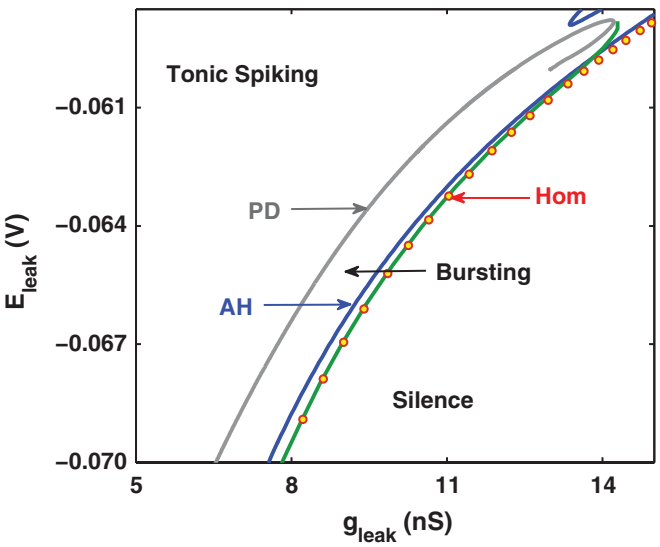

FIG. 6. (Color) Bifurcation diagram of the oscillatory and stationary regimes. The green curve is composed of numerically found points where the transition from bursting activity into silence occurs. The subcritical Andronov-Hopf bifurcation (AH) of the hyperpolarized rest state (silent regime) is shown by the blue curve and marks the boundary where the silent regime loses stability giving rise to the unstable subthreshold oscillations. The red circles correspond to the homoclinic bifurcation (Hom) of the unstable subthreshold oscillations. The area between these two curves (the blue and the red dots) marks the parameter regime where unstable subthreshold oscillations exist. The gray curve marks the period-doubling bifurcation (PD) of large amplitude periodic spiking and marks the transition from tonic spiking to bursting activity. The area of bursting activity is located between the PD and green curves.

periodic orbit representing tonic spiking activity determines the critical values of the controlling parameters, which describe the transition from spiking into bursting. It marks the beginning of the cascade of period-doubling bifurcations transforming the periodic tonic spiking into chaotic tonic spiking. These events occur in a very narrow range of parameters of the leak current. Within a small parameter range bursting coexists with tonic spiking. The mechanism underlying this transition and coexistence has been described for the Hindmarsh-Rose model [30]. Here, we explored the transition from bursting into silence and the mechanism supporting bistability of these two regimes. Based on the knowledge that the range of parameters where unstable subthreshold oscillations exist is bounded between the Andronov-Hopf and homoclinic bifurcations, first, we computed the AH curve in (g_{leak}, E_{leak}) parameter space. Then, in order to locate the homoclinic bifurcation curve (Hom), we increased g_{leak} while following the saddle periodic orbit. We started at the Andronov-Hopf bifurcation where the orbit appeared and followed the orbit until its period became very large, 100 sec, near the homoclinic bifurcation. CONTENT software allows tracking the periodic orbit with the given value of the period; we used g_{leak} and E_{leak} as the two parameters to find the curve with a fixed period of 100 sec. This curve gives a good estimation for the bifurcation values determining the homoclinic bifurcation. The estimated bifurcation values are shown by the red circles in Fig. 6. One can see that the detected points representing the homoclinic bifurcation of the unstable periodic orbit match well with the border between bursting and silence calculated previously by numerical simulations [24]. Hence, the transition from bursting activity into silence is associated with the homoclinic bifurcation, and the range of bistability in leak current parameter space is limited by the subcritical Andronov-Hopf and homoclinic bifurcations for the saddle periodic orbit.

III. DISCUSSION

In a single neuron, interplay between different ionic currents can lead to the coexistence of different regimes of activity, such as tonic spiking, bursting, silence, and subthreshold oscillations. The documented types of bistability include coexistence of bursting and tonic spiking [12,14,24,31], depolarized and hyperpolarized silent states [3,32], two tonic spiking regimes [33], tonic spiking and silence [6], and different patterns of bursting [14,24,34]. Although bistability as a phenomenon has been shown in many different neuronal systems, the biophysical mechanisms supporting bistability are largely not known.

The coexistence of tonic spiking and silence has been particularly extensively studied [19]. It was detected in various types of neurons, from spinal motoneurons to neuronal networks of the entorhinal cortex, and thalamocortical network [1–3,35]. Bistability has been found to occur spontaneously or to be induced by neuromodulators. For example, spontaneous bistability was demonstrated in Purkinje cells in the rat and guinea pig [4]. Turtle and cat motoneurons become bistable after modulation of membrane properties by serotonin [3,36]. Analysis of neuronal Hodgkin-Huxley type models exhibiting coexistence of tonic spiking and silence suggests two main types: i) The depolarized tonic spiking regime and rest state are

separated by the stable manifold of a saddle equilibrium [20]; and ii) the trajectory of the tonic spiking of larger amplitude goes around the hyperpolarized rest state so that the states are separated by the stable manifold of a saddle periodic orbit [6,16,17,19]. The second type features Rinzel's mechanisms of bistability. The mechanism of bistability described in this paper is of the second type, except that the bursting state is in the place of tonic spiking.

A saddle periodic orbit is a generic component of a number of mechanisms supporting bistability in the dynamics of single neurons [6,17,19,31,33,37,38]. Its stable manifold acts as a threshold between the two regimes; and different perturbations of the state of the model could induce crossing the threshold and a switch from one regime to the other. Analysis of the process of switching between regimes of activity with noise or pulses of injected current applied to a bistable neuron or network is a valuable tool for the investigation of bistability [6,16–18].

After the separating regime is identified, an essential part of the description of a mechanism supporting bistability is the description of the appearance and disappearance of the regime under variation of a controlling parameter. This description allows one to identify the factors that cause the bistability and the range of the parameter values supporting it. The choice of parameter is usually dictated by the topic of study. The bifurcation theory provides appropriate tools for this task. For the Hodgkin-Huxley model, the Rinzel mechanism determines that the unstable orbit appears through the Andronov-Hopf bifurcation and disappears through the saddle-node bifurcation for periodic orbits as the polarizing current is varied [19]. The Hodgkin-Huxley model was also analyzed under variation of the concentration of K^+, which affects the membrane potential in accordance with the Nernst potential. This analysis was motivated by the hypothesis that the elevation of external K^+ concentration can induce seizures. The analysis shows the same mechanism of bistability [17].

By applying the bifurcation analysis to the model of the leech heart interneuron, we showed that for a given value of E_{leak} the stable hyperpolarized equilibrium and bursting regime coexisted in a certain range of values of g_{leak}. For a smaller g_{leak}, this range is limited by the subcritical Andronov-Hopf bifurcation at which the unstable periodic orbit appears. In this regard, the orbit appears in accordance with the Rinzel mechanism of the coexistence of tonic spiking and silence. For a larger g_{leak}, the range of bistability is limited by the homoclinic bifurcation of a periodic orbit. The latter distinguishes the mechanism presented here from the Rinzel mechanism, which has the unstable orbit ceasing at the saddle-node bifurcation for periodic orbits. Outside of the above-mentioned range, bistability of bursting and silence was not observed. We performed two-parameter bifurcation analysis to trace the Andronov-Hopf and homoclinic bifurcations using the leak current parameters as the bifurcation parameters and placed them on the bifurcation diagram obtained previously [24]. On this diagram, we showed that the transition from bursting to silence approximately coincides with the two-parameter curve of the homoclinic bifurcation (Fig. 6). This type of analysis of biophysically realistic models could provide help establishing the origin and roles of bistability in the functioning of the nervous system.

Similarly to electronic and other technical devices, in neuronal networks the bistable neurons could play the roles of switch, relay, logic, and memory elements [39]. In the realm of motor control, bistable neurons appear to be a natural choice as elements of multifunctional central pattern generators so that the same network can generate several behavioral patterns [40–42]. In contrast to multifunctional central pattern generators, for the leech heartbeat central pattern generator bistability in the leech heart interneurons seems to be a pathological, life threatening phenomenon. This study predicts the existence of bistability of the leech heart interneuron under conditions leading to elevated conductance of the leak current.

Bistability of a nervous system affected by a pathological condition like seizures coexisting with an alternative, functional regime could be the key element determining the seizure dynamics [7,8,43]. If seizure activity coexists with a functional state, then based on the theory of bistability one could create a feedback procedure to switch it back from seizure. Stimulation by noise of a neuronal network was tested to reduce the duration of seizure episodes [7,8]. In the case of Parkinson's disease, theoretical analysis of the coexistence of pathological synchronization and functional desynchronized states helps in the designing of deep brain stimulation techniques that promote antikindling and desynchronization of the network, suppressing the pathological activity by electric stimulation [10,44].

ACKNOWLEDGMENTS

This work was supported by NSF Grant No. PHY-0750456 to G.C. and the Brains and Behavior program of Georgia State University, Atlanta, Georgia. We thank W. Barnett for carefully reading the manuscript.

APPENDIX: MODEL

$$
\begin{aligned}
CV' = &-[\bar{g}_{\text{Na}} m_{\text{Na}}^3 h_{\text{Na}} (V - E_{\text{Na}}) \\
&+ \bar{g}_{\text{P}} m_{\text{P}} (V - E_{\text{Na}}) \\
&+ \bar{g}_{\text{K1}} m_{\text{K1}}^2 h_{\text{K1}} (V - E_{\text{K}}) \\
&+ \bar{g}_{\text{K2}} m_{\text{K2}}^2 (V - E_{\text{K}}) \\
&+ \bar{g}_{\text{KA}} m_{\text{KA}}^2 h_{\text{KA}} (V - E_{\text{K}}) \\
&+ \bar{g}_{\text{CaS}} m_{\text{CaS}}^2 h_{\text{CaS}} (V - E_{\text{Ca}}) \\
&+ \bar{g}_{\text{CaF}} m_{\text{CaF}}^2 h_{\text{CaF}} (V - E_{\text{Ca}}) \\
&+ \bar{g}_{\text{h}} m_{\text{h}}^2 (V - E_{\text{h}}) \\
&+ g_{\text{leak}} (V - E_{\text{leak}})], \\
m'_{\text{Na}} = &\frac{\left[f_{m\text{Na}}^{\infty}(-150.,0.029,V) - m_{\text{Na}} \right]}{0.0001}, \\
h'_{\text{Na}} = &\frac{\left[f_{h\text{Na}}^{\infty}(500.,0.03,V) - h_{\text{Na}} \right]}{\tau_{Na}(V)}, \\
m'_{P} = &\frac{\left[f_{mP}^{\infty}(-120.,0.039,V) - m_{\text{P}} \right]}{\tau(400,0.057,0.01,0.2,V)}, \\
m'_{\text{CaS}} = &\frac{\left[f_{m\text{CaS}}^{\infty}(-420.,0.0472,V) - m_{\text{CaS}} \right]}{\tau(-400,0.0487,0.005,0.134,V)},
\end{aligned}
$$

$$h'_{\mathrm{CaS}} = \frac{\left[f^{\infty}_{h\mathrm{CaS}}(360.,0.055,V) - h_{\mathrm{CaS}}\right]}{\tau(-250,0.043,0.2,5.25,V)},$$

$$m'_{\mathrm{CaF}} = \frac{\left[f^{\infty}_{m\mathrm{CaF}}(-600.,0.0467,V) - m_{\mathrm{CaF}}\right]}{\tau_{CaF}(V)},$$

$$h'_{\mathrm{CaF}} = \frac{\left[f^{\infty}_{h\mathrm{CaF}}(350.,0.0555,V) - h_{\mathrm{CaF}}\right]}{\tau(270,0.055,0.06,0.31,V)},$$

$$m'_{\mathrm{K1}} = \frac{\left[f^{\infty}_{m\mathrm{K1}}(-143.,0.021,V) - m_{\mathrm{K1}}\right]}{\tau(150,0.016,0.001,0.011,V)},$$

$$h'_{\mathrm{K1}} = \frac{\left[f^{\infty}_{h\mathrm{K1}}(111.,0.028,V) - h_{\mathrm{K1}}\right]}{\tau(-143,0.013,0.5,0.2,V)},$$

$$m'_{\mathrm{K2}} = \frac{\left[f^{\infty}_{m\mathrm{K2}}(-83.,0.02,V) - m_{\mathrm{K2}}\right]}{\tau(200,0.035,0.057,0.043,V)},$$

$$m'_{\mathrm{KA}} = \frac{\left[f^{\infty}_{m\mathrm{KA}}(-130.,0.044,V) - m_{\mathrm{KA}}\right]}{\tau(200,0.03,0.005,0.011,V)},$$

$$h'_{\mathrm{KA}} = \frac{\left[f^{\infty}_{h\mathrm{KA}}(160,0.063,V) - h_{\mathrm{KA}}\right]}{\tau(-300,0.055,0.026,0.0085,V)},$$

$$m'_{h} = \frac{\left[f^{\infty}_{h}(V) - m_{\mathrm{h}}\right]}{\tau(-100,0.073,0.7,1.7,V)},$$

where the reversal potentials and maximal conductances of the ionic currents are $E_{\mathrm{Na}} = 0.045V$, $E_{\mathrm{K}} = -0.07V$, $E_{\mathrm{Ca}} = 0.135V$, $E_h = -0.021V$, $\bar{g}_{\mathrm{Na}} = 200$ nS, $\bar{g}_{\mathrm{P}} = 7$ nS, $\bar{g}_{\mathrm{CaS}} = 3.2$ nS, $\bar{g}_{\mathrm{CaF}} = 5$ nS, $\bar{g}_{\mathrm{K1}} = 100$ nS, $\bar{g}_{\mathrm{K2}} = 80$ nS, $\bar{g}_{\mathrm{KA}} = 80$ nS, $\bar{g}_h = 4$ nS. The cell membrane capacitance C is 0.5 nF. The steady-state activation and inactivation functions are defined by $f^{\infty}_{x}(a,b,V) = 1/[1 + e^{a(V+b)}]$, where x defines the gating variable. The steady-state activation function of the hyperpolarization activated current, the inactivation time constants of the fast sodium and calcium currents, and the time constants of the activation and inactivation variables of the other currents are given by

$$f^{\infty}_{h}(V) = \frac{1}{1 + 2e^{180[V+0.047]} + e^{500[V+0.047]}},$$

$$\tau_{\mathrm{Na}}(V) = 0.004 + \frac{0.006}{1 + e^{500[V+0.028]}} + \frac{0.01}{\cosh(300[\mathrm{V} + 0.027])},$$

$$\tau_{\mathrm{CaF}}(V) = 0.011 + \frac{0.024}{\cosh(-330[\mathrm{V} + 0.0467])},$$

$$\tau(a,b,c,d,V) = c + \frac{d}{1 + e^{a[V+b]}}.$$

[1] P. Fuentealba, I. Timofeev, M. Bazhenov, T. Sejnowski, and M. Steriade, J. Neurophysiol. **93**, 294 (2005).
[2] A. Egorov, B. Hamam, E. Fransén, M. Hasselmo, and A. Alonso, Nature (London) **420**, 173 (2002).
[3] J. Hounsgaard and O. Kiehn, J. Physiol. **414**, 265 (1989).
[4] Y. Loewenstein, S. Mahon, P. Chadderton, K. Kitamura, H. Sompolinsky, Y. Yarom, and M. Häusser, Nature Neurosci. **8**, 202 (2005).
[5] J. Jalife and C. Antzelevitch, Science **206**, 695 (1979).
[6] R. Guttman, S. Lewis, and J. Rinzel, J. Physiol. **305**, 377 (1980).
[7] J. Foss and J. Milton, in *Epilepsy as a Dynamic Disease*, edited by J. Milton and P. Jung, Vol. 16 (Springer, Berlin, 2003), p. 283.
[8] P. Suffczynski, S. Kalitzin, and F. H. Lopes da Silva, Neuroscience. **126**, 467 (2004).
[9] D. Durand, A. Jensen, and M. Bikson, in *Proceedings of the International Conference of the IEEE Engineering in Medicine and Biology Society, 2006*, Vol. 1 (IEEE, Piscataway, New Jersey, 2006), p. 1624.
[10] P. A. Tass and C. Hauptmann, Int. J. Psychophysiol. **64**, 55 (2007).
[11] E. Marder and R. Calabrese, Physiol. Rev. **76**, 687 (1996).
[12] H. Lechner, D. Baxter, J. Clark, and J. Byrne, J. Neurophysiol. **75**, 957 (1996).
[13] F. Nadim, Y. Manor, N. Kopell, and E. Marder, Proc. Natl. Acad. Sci. USA **96**, 8206 (1999).
[14] C. Canavier, D. Baxter, J. Clark, and J. Byrne, J. Neurophysiol. **72**, 872 (1994).
[15] A. Hodgkin and A. Huxley, J. Physiol. **117**, 500 (1952).
[16] B. Gutkin, J. Jost, and H. Tuckwell, Naturwissenschaften **96**, 1091 (2009).
[17] P. Hahn and D. Durand, J. Comput. Neurosci. **11**, 5 (2001).
[18] D. Paydafar, D. Forger, and J. Clay, J. Neurophysiol. **96**, 3338 (2006).
[19] J. Rinzel, Federation Proc. **37**, 2793 (1978).
[20] E. Izhikevich, *Dynamical Systems in Neuroscience: The Geometry of Excitability and Bursting* (MIT Press, Cambridge, Massachusetts, 2007).
[21] J. Schmidt and R. Calabrese, J. Exp. Biol. **171**, 329 (1992).
[22] R. Calabrese, F. Nadim, and H. Olsen, J. Neurobiol. **27**, 390 (1995).
[23] A. Hill, J. Lu, M. Masino, O. Olsen, and R. Calabrese, J. Comput. Neurosci. **10**, 281 (2001).
[24] G. Cymbalyuk, Q. Gaudry, M. Masino, and R. Calabrese, J. Neurosci. **22**, 10580 (2002).
[25] CONTENT is freely available at [http://www.staff.science.uu.nl/kouzn101/CONTENT/].
[26] A. I. Khibnik, Yu. A. Kuznetsov, V. V. Levitin, and E. V. Nikolaev, Physica D **62**, 360 (1993).
[27] L. Lapicque, J. Physiol. Pathol. Gen. **9**, 620 (1907).
[28] H. A. Blair, J. Gen. Physiol. **15**, 709 (1932).
[29] N. Brunel and M. C. W. van Rossum, Biol. Cybern. **97**, 337 (2007).
[30] A. Shilnikov and M. Kolomiets, Int. J. Bif. Chaos **18**, 1 (2008).
[31] F. Fröhlich and M. Bazhenov, Phys. Rev. E **74**, 031922 (2006).
[32] V. Crunelli, T. Toth, D. Cope, K. Blethyn, and S. Hughes, J. Physiol. **562**, 121 (2005).
[33] G. Cymbalyuk and A. Shilnikov, J. Comput. Neurosci. **18**, 255 (2005).
[34] R. Butera, Chaos **8**, 274 (1998).
[35] S. Williams, S. Christensen, G. Stuart, and M. Häusser, J. Physiol. **539**, 469 (2002).
[36] J. Perrier and J. Hounsgaard, Brain Res. Bull. **53**, 529 (2000).

[37] J. Cressman, G. Ullah, J. Ziburkus, S. Schiff, and E. Barreto, J. Comput. Neurosci. **26**, 159 (2009).
[38] A. Shilnikov, R. L. Calabrese, and G. Cymbalyuk, Phys. Rev. E **71**, 056214 (2005).
[39] E. Marder, L. Abbott, G. Turrigiano, Z. Liu, and J. Golowasch, Proc. Natl. Acad. Sci. USA **93**, 13481 (1996).
[40] K. Briggman and W. Kristan, Annu. Rev. Neurosci. **31**, 271 (2008).
[41] S. Venugopal, J. Travers, and D. Terman, J. Comput. Neurosci. **22**, 223 (2007).
[42] A. Shilnikov, R. Gordon, and I. Belykh, Chaos **18**, 037120 (2008).
[43] D. Takeshita, Y. D. Sato, and S. Bahar, Phys. Rev. E **75**, 051925 (2007).
[44] Y. L. Maistrenko, B. Lysyansky, C. Hauptmann, O. Burylko, and P. A. Tass, Phys. Rev. E **75**, 066207 (2007).